

Chapter 2

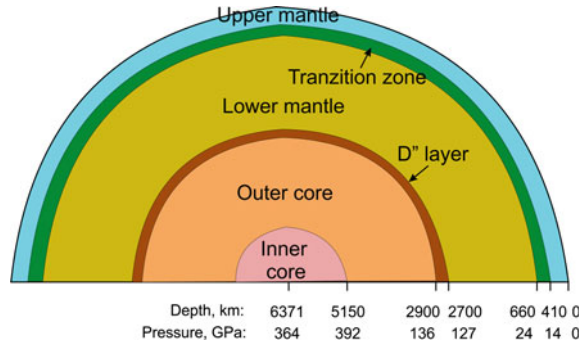
General Physical and Chemical Models of the Earth's Lower Mantle

Abstract The most popular model of the lower mantle is the Preliminary Reference Earth Model (PREM), derived from seismic observations assuming the pyrolitic composition of the lower mantle. The uppermost part of the lower mantle (~ 660 – 770 km deep) has a steep velocity gradient, reflecting the mineral structure transformation from ringwoodite to bridgmanite and ferropericlase, after which gradual increase in both the compressional velocity (V_p) and shear velocity (V_s) reflects the near adiabatic compression of mineral phases. The adiabatic geothermal gradient within the upper mantle decreases with increasing depth without phase transitions. Subducting lithospheric slabs may significantly cool temperature profiles, particularly in the upper part of the lower mantle. However, results of experiments on the density of natural peridotite, performed within the range of entire lower-mantle pressures along the geotherm, demonstrated their significant mismatch with the PREM density model. This implies that the upper and the lower mantle must have different chemical compositions, i.e. the mantle is chemically stratified, with the inference of a non-pyrolitic composition of the lower mantle. The diapason of oxygen fugacity within the entire sequence of lower-mantle region may reach ten logarithmic units, varying from below the IW buffer to the FMQ buffer values.

2.1 General

In one of the first geophysical models of the Earth, Bullen (1942) proposed a spherically symmetric ‘shell model’ of the Earth’s interior and distinguished eight layers labelled alphabetically from A to G, with the crust as the A layer, the upper mantle as the B layer, the transition zone as the C layer, the entire lower mantle as the D layer, the outer core as the E layer, its lower part as the F layer, and the inner core as the G layer. Later, Bullen found the D layer to be made from two different layers: the upper part of the D layer, about 1800 km thick, was renamed D’; and the lower part (the bottom 200 km) was named D’’ (Bullen 1950). To date, only the

Fig. 2.1 General structure of the Earth. Borders of the major Earth's regions and corresponding pressure values, accepted in this work, are shown at the bottom



latter name is in use to refer to the lowermost 200 km of the mantle, which may be considered to be a boundary transitional layer from the lower mantle to the outer core (Fig. 2.1).

Later seismic studies revealed more complex regions of the Earth and the following principal regions were identified within the Earth, based on seismic parameters (Dziewonski and Anderson 1981).

1. Ocean layer.
2. Upper and lower crust.
3. Region above the low velocity zone (LVZ), starting at a depth of 220 km.
4. LVZ (80–220 km depth).
5. Region between the LVZ and 400 km discontinuity.
6. Transition zone (TZ), spanning the region between the 400 and 670 km discontinuities.
7. Lower mantle, subdivided into three parts by second-order discontinuities at 770, 2740 and 2740 km. The lowermost part corresponds to the D'' layer.
8. Outer core (2890–5150 km).
9. Inner core (5150–6371 km).

These depth estimates are slightly corrected in modern petrological constructions (e.g., the upper and lower borders of the TZ at 410 and 660 km, respectively, with the borders of the D'' layer at 2700 and 2900 km). The generalized structure of the Earth accepted in this work is presented in Fig. 2.1.

2.2 Seismic Velocities in the Lower Mantle

The decision to distinguish the boundary at ~ 660 –670 km between the lower mantle and the transition zone is based on seismologic data, according to which remarkable changes (6–11%) in the velocities of seismic waves occur at this depth (Preliminary Reference Earth Model or PREM; Dziewonski and Anderson 1981). The exact position of this seismic discontinuity varies depending on the tectonic

position of the area. It is located deeper than 670 km under subduction zones and shallower at ‘hotspot’ areas, such as Iceland, Hawaii and others (e.g., Shen et al. 1998). The increasing proportion of the basaltic component within the lower mantle in these areas may stimulate depth of this border to increase to 720 km (Deuss et al. 2006). In some areas, it bifurcates to 520 and 670 km boundaries (e.g., Deuss and Woodhouse 2001). In addition, undulation of the upper boundary of the lower mantle may be caused by the presence of high proportions of volatile components (such as water) and Mg–Fe partitioning between coexisting mineral phases in the constituent materials. The most popular 1D Earth model, PREM, is presented in Fig. 2.2.

The uppermost part of the lower mantle (~ 660 – 770 km deep) has a steep velocity gradient, reflecting the mineral structure transformation from ringwoodite to bridgmanite and ferropericlase. After that, there is a gradual increase in both the compressional velocity (V_p) and shear velocity (V_s), reflecting the near adiabatic compression of mineral phases (Dziewonski and Anderson 1981). In the normal lower mantle, three major minerals are present: bridgmanite, ferropericlase and CaSi-perovskite; stishovite can also be present. The velocities of each mineral phase vary with pressure and equilibrium composition in response to partitioning of components among phases. Comparison of the sound velocities of these phases shows that the fastest mantle phase is stishovite; however, the lowermost part of the

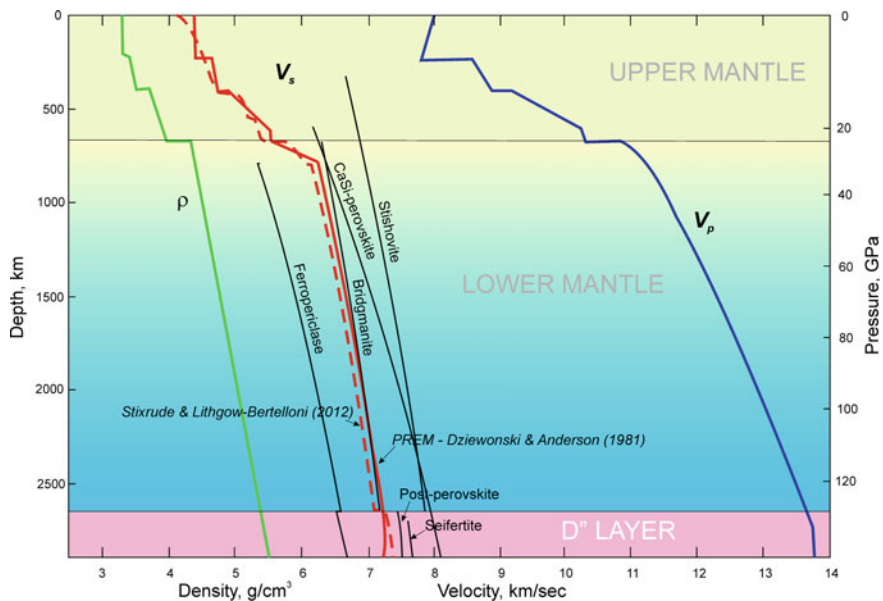


Fig. 2.2 Pyrolite mantle seismic wave velocity and density profiles as a function of depth. V_p compressional wave velocity, blue; V_s shear-wave velocity, red; velocities of the major lower-mantle minerals, black; ρ density of pyrolite in g/cm^3 , green. Data from Dziewonski and Anderson (1981) and Stixrude and Litgow-Bertelloni (2012)

mantle shows CaSi-perovskite to be faster (Stixrude and Litgow-Bertelloni 2012; Fig. 1.2). Since the seismic wavelength is much greater than the size of the mineral grains, seismic waves see an averaged aggregate of constituent materials. However, lattice preferred orientations of the minerals due to the flow patterns of the mantle can cause seismic heterogeneities. The relative proportions of phases and their compositions may vary; in this case, one should expect additional variations in seismic velocities. However, in the PREM, seismic parameters are distributed homogeneously through the lower mantle, suggesting that the constituent minerals are gravitationally, almost adiabatically compressed, with the exception of the lowermost part of the lower mantle (the D'' layer), where a number of seismic anomalies have been identified (Dziewonski and Anderson 1981; Kennett et al. 1995).

Since the publication of the PREM in 1981, a number of other seismic models have been reported including *isp91* (Kennett and England 1991), AK135 (Kennett et al. 1995), STW105 (Kustowski et al. 2008), GyPSuM (Simmons et al. 2010), and SPani (Tesoniero et al. 2015), amongst others; some of these models mainly focus on specific regions. Furthermore, some of these models deviate from PREM, showing that a re-evaluation of the PREM or a non-pyrolitic lower-mantle composition is needed.

One of most serious challenges to the one-dimensionally homogeneous seismic models such as the PREM has been the consequences of the spin crossover of iron in two major lower-mantle mineral phases, ferropericlase and bridgmanite, which were discovered in the early 2000s (Badro et al. 2003). These minerals have significant iron contents, which can undergo a high-spin to low-spin transition and, as a result, change iron partitioning at relevant pressure–temperature (P – T) conditions of the lower mantle that can affect the physics and chemistry of the host minerals (e.g., Irfune et al. 2010; Lin et al. 2013) (see Chap. 8 for details). Shahnas et al. (2011) evaluated the influence of the iron spin crossover in the lower-mantle minerals on the PREM and found out that spin crossover in the lower mantle above the 1800 km depth does not influence mantle layering significantly. Below this horizon, there is a hot layer, which acquires spin-induced positive buoyancy and which assists in preventing the cold downwelling from penetrating through the 1800 km depth horizon (Shahnas et al. 2011).

2.3 Density Profile

The density profile within the lower mantle, according to the PREM, after jumps related to the olivine \rightarrow wadsleyite \rightarrow ringwoodite \rightarrow bridgmanite + ferropericlase phase transitions, becomes $\sim 4.4 \text{ g/cm}^3$ at the top of the lower mantle, and then increases gradually to $\sim 5.5 \text{ g/cm}^3$ at the mantle/core boundary (Fig. 2.2), mostly because of the compression of the mantle material (assuming the homogeneity of the material and adiabatic character of the process). However, even the early calculations demonstrated that the model composition of the lower mantle is at

least 2.6% less dense than the observed lower-mantle density over the depth range 1000–2000 km; hence, the mantle should be stratified with the layers possibly intermixing (Jeanloz and Knittle 1989). The results of later experiments with a natural peridotite performed entirely within the range of lower-mantle pressures of up to 112 GPa along the geotherm, demonstrated the significant mismatch of density with the PREM density model, particularly in the slopes between the two profiles (Ricolleau et al. 2008, 2009). *This implies that the upper and the lower mantle must have different chemical compositions, i.e., the mantle is chemically stratified, if one uses the PREM as a reference. In that case, the data favour a Si-enriched, less dense lower mantle.*

Ricolleau et al. (2009) calculated that, in order to match their experimentally determined density profile of a pyrolite mantle composition to PREM, the temperature at the top of the lower mantle has to be $\sim 1500 \pm 60$ K, which is ~ 400 K lower than the estimated temperature at a depth of 660 km (Hirose 2002; Katsura et al. 2010) with a superadiabatic geotherm of gradient 0.60 K/km through the lower mantle, which is in disagreement with the adiabatic geotherm (see Sect. 2.5). The measured density for an ultramafic mantle along the geotherm shows a significant mismatch (2%) with the PREM derived from seismic observations assuming pyrolitic composition of the lower mantle. *This points to the likelihood of a non-pyrolitic composition of the lower mantle.*

2.4 Compositional Models and Chemical Homogeneity/Heterogeneity of the Lower Mantle

Knowing the composition of the lower mantle heavily depends on our understanding of the evolution and dynamics of the planet. The Earth's lower mantle is clearly layered with distinct seismic features that separate it from the overlaying upper mantle and transition zone, as well as the underlying outer core. Geochemical studies of the upper mantle materials (especially from xenoliths) show that the upper mantle is mostly made of peridotite with olivine, pyroxene and garnet being the abundant minerals. Together with petrological experiments, Ringwood (1975) proposed that the mantle is made of pyrolite, a hypothetical rock made of peridotite and basalt in a ratio of approximately 3:1. The question for the lower-mantle composition is whether or not the whole mantle remains chemically homogeneous or whether it is layered?

One key parameter in categorizing the composition of the mantle is the Mg/Si ratio that varies from approximately 1 in the chondritic composition model to 1.3 in the pyrolitic model (e.g., Ringwood 1975; Anderson 1983; Hart and Zindler 1986; Javoy 1995). As a simple reference, the Mg/Si ratio is 2 for forsterite (Mg_2SiO_4) and 1 for enstatite and bridgmanite (MgSiO_3). Petrological evidence obtained from the compositional trends in upper mantle peridotites suggests that the Mg/Si ratio of the bulk silicate Earth is close to 1.27, indicating that the upper and lower mantle are homogeneous in composition (Ringwood 1975; Anderson 1983). In the

pyrolitic compositional model of the mantle, the lower mantle is suggested to be made of 75 vol.% bridgmanite [(Mg, Fe) (Al, Si)O₃], 17 vol.% ferropericlase [(Mg, Fe)O], and approximately 8 vol.% CaSiO₃-perovskite (Ringwood 1975). If the Earth was accreted from chondritic meteorites such as the CI chondrites, which have the Mg/Si ratio of approximately 1.074, the lower mantle should be chemically distinct from the upper mantle (e.g., Morgan and Anders 1980; Bass and Anderson 1984; Hart and Zindler 1986; Javoy 1995; McDonough and Sun 1995; Williams and Knittle 2005). The lower mantle in a chondritic compositional model is expected to be enriched in bridgmanite and CaSi-perovskite, with an Mg/Si ratio close to 1 (Anderson 1989).

From a geophysical perspective, a comparison of the seismic profiles with velocity and density profiles of candidate mantle minerals at relevant P - T conditions provides another means by which to evaluate the composition and mineralogy of the lower mantle. For example, Irifune et al. (2010) obtained the velocity profiles of pyrolite and piclogite compositions in a multi-anvil apparatus in transition zone conditions, showing that the velocity and density profiles of the region are most consistent with a pyrolite composition, instead of more pyroxene and garnet-rich piclogite. For the lower mantle, experimental results are rather more scattered because of the technical difficulties in reaching extreme P - T conditions and simultaneously measuring the elasticity of candidate minerals in the region (e.g., Murakami et al. 2012). Theoretical studies using first-principle methods to model the density and velocities of the lower mantle in various compositions conclude that lower mantle with a pyrolitic composition has density and velocity profiles matching the seismic PREM (Wang et al. 2015). Matas et al. (2007) studied the problem of obtaining the thermal structure and bulk chemical composition of the lower mantle from its seismologically determined velocity and density profiles, using the results on the elastic properties of the lower-mantle phases (including, of particular importance, shear moduli). They show the reverse that *these properties do not match the uniform chemical composition model of the lower mantle*. In order to satisfy the 1D seismic profiles, the averaged lower-mantle Mg/Si ratio should be lower than would be usually accepted in the pyrolite model. Instead, there should be a depth-dependent bulk composition with an Mg/Si ratio decreasing from 1.18 ± 0.14 to 1.03 ± 0.16 (i.e., the *increase of Si component to a more chondritic composition*) between 800 and 2700 km. Murakami et al. (2012) measured shear wave velocity and density profiles of bridgmanite and ferropericlase at high P - T using Brillouin spectroscopy and X-ray diffraction, concluding that the lower mantle is mostly made of bridgmanite, named the perovskitic lower mantle.

On the other hand, recent modelling of the shear wave velocity profile, utilizing the third-order Eulerian finite-strain equation, demonstrated that the lower mantle shear wave velocities can resolve PREM for a pyrolitic composition to within 1%. In addition, isotopic fractionation modelling of the $^{143}\text{Nd}/^{144}\text{Nd}$ and $^{176}\text{Hf}/^{177}\text{Hf}$ systems led to the conclusion that an Si-enriched lower mantle, if crystallized from the ancient magma ocean, was not preserved throughout the Earth's history and no longer exists (Hyng et al. 2016). In this model, which supports the idea that the Earth's lower mantle is pyrolitic, the mantle as a whole needs to be chemically

stratified. However, the compositional heterogeneity of the mantle on the basis of modelled seismic velocity profiles were comprehensively studied by Stixrude and Lithgow-Bertelloni (2012). They demonstrated that chemical heterogeneity may survive in the mantle for as long as the age of the Earth because chemical diffusion is inefficient. Estimates of the rate of subduction and mantle processing over geologic history indicate that almost the entire mantle may be composed of lithologically heterogeneous material. The fastest lithology is silica, the presence of which causes the increase in the velocity within the lower mantle (see Sect. 4.6).

However, it should be noted that considering limited experimental constraints on the elasticity and sound velocity of lower mantle minerals at P – T conditions relevant to the lower mantle, recent theoretical models using new ρ and V_ϕ profiles concluded that predictions for a pyrolitic composition of the lower mantle have seismic properties in agreement with the PREM (Wang et al. 2015; Sun et al. 2016; Zhang et al. 2016).

2.5 Geotherm

Temperature distribution in the Earth's interior reflects the energy balance between heat generation and dissipation. The heat source in the mantle is believed to be mostly primordial and radiogenic, while the dissipation is most dominant through convection, but radiative conduction can also play a certain role. However, there is no direct way to measure temperature in the Earth's deep interior, except with some drilled boreholes as deep as approximately 10 km. A combination of indirect methods was used to estimate the temperature distribution in the deep mantle (Brown and Shankland 1981; Ito and Katsura 1989; da Silva et al. 2000; Stacey and Davis 2008; Katsura et al. 2010).

In most geotherm models of the Earth, conductive and radiative heat transfer is considered to be negligible because of the small thermal conductivity of mantle minerals, and heat should be effectively transported by convection into most parts of the mantle (Katsura et al. 2010). Therefore, the temperature gradient is considered to be nearly adiabatic in the Earth's mantle. The adiabatic temperature gradient $(\partial T/\partial z)_s$ is expressed as:

$$(\partial T/\partial z)_s = \alpha g T / C_p;$$

where T is temperature, z is depth, g is gravitational acceleration, α and C_p are the thermal expansion coefficient and isobaric heat capacity of the constituent materials, respectively (Turcotte and Schubert 2002). Using this equation, one can calculate the temperature gradient and geotherm if the aforementioned thermodynamic parameters and a reference temperature at a given depth are known.

Based on the estimated maximal temperature of the olivine–wadsleyite transition at the 410 km seismic discontinuity of 1830 ± 48 K, Katsura et al. (2010) calculated the adiabatic temperature profile for the entire mantle using experimentally

measured thermal expansion coefficients of the mantle minerals with the known gravity accelerations and the assumption that the whole mantle has a constant pyrolytic composition based on the whole mantle convection model (Stacey and Davis 2008). The thermal expansion coefficient is the most critical parameter for the adiabatic geotherm. In the lower mantle, it gradually decreases in pyrolytic composition from $3 \times 10^{-5}/\text{K}$ at the topmost lower mantle to $1 \times 10^{-5}/\text{K}$ to lowermost lower mantle. The adiabatic geothermal gradient within the upper mantle shows the same tendency as the thermal expansion coefficient. It decreases with increasing depth without phase transitions, but can potentially increase across phase transitions. The geothermal gradient is 0.47 K/km at the top of the lower mantle, and decreases to 0.24 K/km at 2600 km in depth (Katsura et al. 2010). In earlier works, it has been suggested to be 0.3 K/km (Brown and Shankland 1981; Turcotte and Schubert 2002), 0.4 K/km and rather constant (Stacey and Davies 2008) and 0.5–0.9 K/km and increasing with depth (Matas et al. 2007).

The temperature profile for the mantle calculated by Katsura et al. (2010) is shown in Fig. 2.3. The temperature at the top of the lower mantle is found to be 1960 ± 50 K, which coincides with earlier estimates by Hirose (2002). The temperature at 2700 km depth is 2630 ± 60 K, if the convective heat transfer still dominates in this region. This temperature profile is 70–110 K higher than that of Ito and Katsura (1989) and Brown and Shankland (1981) because the temperature

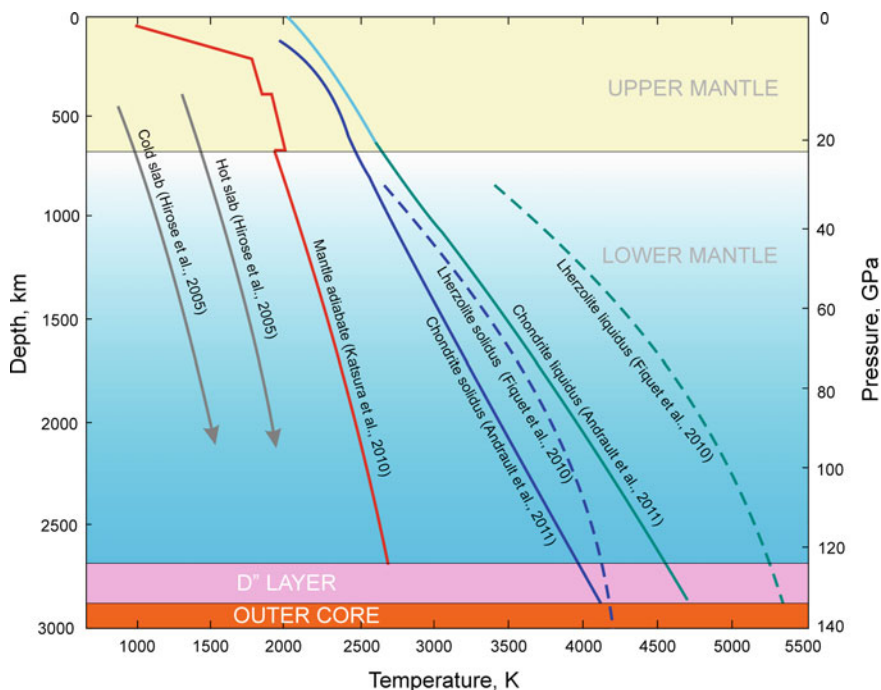


Fig. 2.3 Profiles of temperature, solidus and liquidus in the mantle. Data from Kirby et al. (1996), Katsura et al. (2010), Fiquet et al. (2010) and Andrault et al. (2011)

Table 2.1 Reference temperature at the 660 km depth used in the literature geotherm modelling

| Authors | 660-km phase transition temperature |
|----------------------------|-------------------------------------|
| Brown and Shankland (1981) | 1873 |
| Stacey and Davis (2008) | 1931 |
| Katsura et al. (2010) | 1980 |

at the 660 km discontinuity was estimated to be lower in those studies (Table 2.1). Da Silva et al.'s (2000) temperature profiles are much steeper in the whole lower mantle because the temperature profiles in this study were obtained by matching the modelled elastic wave velocities of the lower mantle minerals with the seismic profiles, under the assumption that the heat must be mainly transferred not by convection, but by conduction.

Subducting lithospheric slabs may significantly cool temperature profiles, particularly in the upper part of the lower mantle. The profiles of both old, faster subducting 'cold' slabs and younger, slower subducting 'hot' slabs after Kirby et al. (1996) are shown in Fig. 2.3.

Experimental data demonstrated that an electronic spin transition in iron, which occurs at mid-mantle depths, results in changes to the physical properties of the ferropericlase, comprising a significant part of the bulk lower mantle. The numerical model demonstrated that as the result of this electronic transition, the lowermost region of the mantle is slightly warmed, whereas the upper mantle is slightly cooled by spin-induced effects (Shahnas et al. 2011).

2.6 Liquidus and Solidus of Mantle Material

The eutectic or peritectic melting of mantle materials consisting of phases with constant and changeable solid solution compositions is characterized by solid and liquid phase relations. Sometimes, the phase relations can be significantly affected by the addition of a small amount of volatiles. Solidus and liquidus profiles within the mantle were mostly established on the basis of high P – T laser-heated diamond-anvil cell (LHDAC) experiments on representative compositions using in situ synchrotron X-ray diffraction measurements and/or quenched sample analysis. Various criteria for detecting melting include diffuse X-ray scattering, melt textures and X-ray microtomographs via edge absorption have been adopted in this area of research (e.g., Fiquet et al. 2010; Andraut et al. 2011; Nomura et al. 2012).

Natural anhydrous fertile lherzolite KLB-1, a natural analogue of the upper mantle (spinel lherzolite from the Kilbourne Hole crater in New Mexico, USA; Davis et al. 2009) was studied to establish its solidus line in the lower mantle (Fiquet et al. 2010). The results show that the solidus line is approximately 900–1200 K higher than the expected adiabatic geotherms, suggested by Brown et al. (1981), within the mid-mantle region at depths of 1300–1700 km and \sim 1400 K higher at the bottom of the lower mantle at a depth of 2700 km. The melting

temperature at the core–mantle boundary (CMB) was established to be at 4180 ± 150 K (Fiquet et al. 2010). These data are in good agreement with the mantle solidus inferred at the CMB conditions from shock wave experiments on $(\text{Mg}_{0.9}\text{Fe}_{0.1})_2\text{SiO}_4$ (Holland and Ahrens 1997) and from first principles molecular dynamics simulations (Stixrude et al. 2009).

Andrault et al. (2011) investigated the melting properties of a synthetic chondritic primitive mantle up to the CMB pressure and found a similar solidus profile; however, the solidus and liquidus chondritic temperatures of 4150 ± 150 K and 4725 ± 150 K, respectively, at the CMB at 2900 km were much lower than for lherzolite. Nomura et al. (2012) indicated that the solidus temperature of a pyrolite composition, which represents an upper boundary for the melting of the primitive lowermost mantle materials, is as low as $3570 \text{ K} \pm 200 \text{ K}$ at the CMB pressures. The low solidus temperature also suggests the melting temperature of the outer core to be much lower than what may have been expected previously.

Although the studied compositions may differ from the real lower-mantle composition, the obtained results may be used as approximations.

2.7 Oxidation Potential in the Lower Mantle

2.7.1 General

Oxygen fugacity f_{O_2} (the chemical potential of oxygen) is a fundamental thermodynamic parameter in the growth and stability of mineral phases formed in the Earth's mantle. Oxygen fugacity can influence phase relations, the presence and speciation of a fluid phase, among other things

As an equivalent of the partial pressure of oxygen in a particular environment (melts, rocks, etc.), oxygen fugacity is measured in pascals (Pa). After recalculation in logarithmic units, it is usually compared with the value, corresponding (at given P – T values) to the f_{O_2} value of the fayalite-magnetite-quartz (FMQ) or iron-wüstite (IW) buffer values, corresponding to reactions $3\text{Fe}_2\text{SiO}_4 + \text{O}_2 = 2\text{Fe}_3\text{O}_4 + 3\text{SiO}_2$ and $2(1-x)\text{Fe} + \text{O}_2 = 2\text{Fe}_{1-x}\text{O}$, respectively. Usually, mantle values of f_{O_2} are located between or close to FMQ and IW buffer values.

At the top of the upper mantle, the calculated oxygen fugacity is shown to vary between -3 to $+2$ logarithmic units of the FMQ oxygen buffer (Frost and McCammon 2008; Stagno et al. 2013). With increasing depth, f_{O_2} decreases relative to oxygen buffers as a result of elevated pressure controlling $\text{Fe}^{3+}/\text{Fe}^{2+}$ equilibria (Wood et al. 1990). At approximately 8 GPa (~ 250 km depth), f_{O_2} should be 5 log units below FMQ, and at the base of the upper mantle (~ 410 km; 14 GPa) f_{O_2} has been suggested to extend to ~ 0.8 log units below the IW buffer, assuming the precipitation of Ni in bulk silicate Earth at this depth (Frost and McCammon 2008).

This calculated data is supported by direct analyses of $\text{Fe}^{3+}/\Sigma\text{Fe}$ ratios in garnet grains hosted as inclusions within peridotite xenoliths present in South African

(Woodland and Koch 2003; Lazarov et al. 2009; Hanger et al. 2014) and Canadian (McCammon and Kopylova 2004; Creighton et al. 2010) kimberlites. Similar results were obtained from spinel and garnet peridotites in Siberia, demonstrating the decrease of f_{O_2} with increasing pressure: from +1 to $-4\Delta\log f_{\text{O}_2}$ (FMQ) at a depth of 180 km (Goncharov et al. 2012) and from -2.5 to nearly $-5.9\Delta\log f_{\text{O}_2}$ (FMQ) at a depth of 90–220 km (1.2–7.1 GPa pressure) (Yaxley et al. 2012). Local variations in oxygen fugacity within the upper mantle are caused by petrological processes, such as partial melting, mantle metasomatism and the recycling of oxidized material during subduction (Rohrbach and Schmidt 2011; Berry et al. 2013). Controls relating to the local tectonic environment have also been suggested (Foley 2011).

Estimates of oxygen fugacity for the deep mantle suggest that at depths in excess of 250 km (>8 GPa), f_{O_2} becomes narrowly constrained. Given equilibrium between mantle phases with molar $\text{Mg}/(\text{Mg} + \text{Fe}^{2+}) (=X_{\text{Mg}}) < 0.90$ and $(\text{Fe}, \text{Ni})_{\text{metal}}$, f_{O_2} can only vary from values around the IW equilibrium where the metal would be Ni-rich, to about 1.5 log units below IW where the metal would be almost pure iron (Rohrbach and Schmidt 2011). The same range of f_{O_2} variations (between IW and IW-1.5) was supposed for the entire lower mantle, suggesting that the bulk oxygen content of the lower mantle is similar to that of the upper mantle (Frost and McCammon 2008).

Direct measurements of lower-mantle redox conditions, which provide crucial constraints on the real oxidation state of the lower mantle, are scarce. Until recently, less than 20 grains of ferropericlasite, bridgmanite and jeffbenite from São Luiz (Brazil) and Kankan (Guinea) placer deposits have been analysed by means of Mössbauer spectroscopy to determine their $\text{Fe}^{3+}/\Sigma\text{Fe}$ ratios (McCammon et al. 1997, 2004b). The results demonstrate the small amount of Fe^{3+} in ferropericlasite ($\text{Fe}^{3+}/\Delta\text{Fe} = 0.1\text{--}6.0\%$), which is in direct contrast to the high amounts of Fe^{3+} in bridgmanite (9–75%) and, in particular, in jeffbenite (66–74%). These differences are characteristic even for coexisting phases, and have been considered to reflect differences in the crystal structures. For example, large amounts of Fe^{3+} in bridgmanite and jeffbenite were considered due to the presence of Al in their compositions, which stabilizes Fe^{3+} in the perovskite structure, independent of oxygen fugacity (McCammon 1997; McCammon et al. 2004a). Based on these results, supported by experimental data, the overall picture of redox conditions in the lower mantle was suggested to be a “generally reduced bulk mantle with possibly more oxidised regions, at least some associated with subducting slabs” (McCammon et al. 2004b).

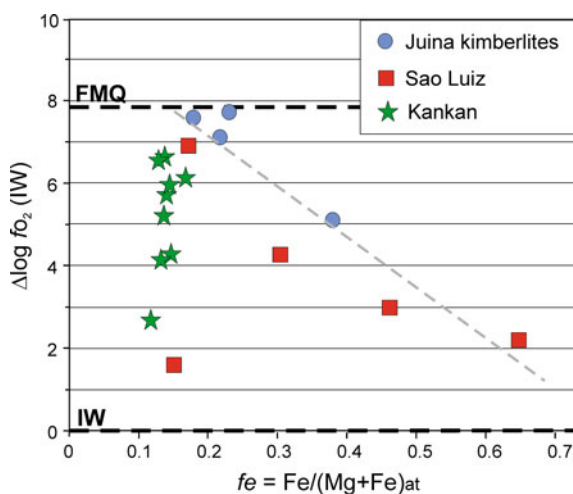
Otsuka et al. (2013) calculated the redox conditions of earlier studies (McCammon et al. 1997, 2004b) for lower-mantle ferropericlasite inclusions in diamond. The $\Delta\log f_{\text{O}_2}$ (IW) values appeared to vary from 4.3–3.3 for Kankan, Guinea and from 3.2–2.6 for São Luiz, i.e. within the total $\Delta = 1.6$ range. The estimated oxygen fugacities are close to the upper stability limit of diamond in mantle peridotite at the top of the lower mantle at adiabatic or slightly superadiabatic temperatures (Otsuka et al. 2013) and lay within a narrow range from 2.6–4.3 log units above the IW buffer ($\Delta = 1.7$ log units), which is lower than expected by Rohrbach and Schmidt (2011), but as ‘narrowly constrained’ as the latter suggested.

Alternative calculations performed by Ryabchikov and Kaminsky (2013, 2014), based upon the calculated Ni/Fe partition coefficient, estimated the variation of $\log f_{\text{O}_2}$ values in the lower mantle (at the pressure conditions from 30–70 GPa) within a much wider range from -1 and -1.5 log units below the IW buffer to $+3$ and $+5$ log units (and even higher, in the presence of carbonates) above the IW buffer ($\Delta \geq 7$ log units). The proof of such great variations of f_{O_2} is the presence (among inclusions in lower-mantle diamonds) of native iron and iron carbides (Kaminsky and Wirth 2011) from one side, and magnesite and other carbonate minerals (Kaminsky et al. 2009, 2013) to the other side. The calculations below are based on Kaminsky et al. (2015).

2.7.2 Oxygen Fugacity Conditions of the Formation of Natural Ferropericlas

Recently, oxygen fugacity conditions in the lower mantle were estimated on the basis of the analysis of ferropericlas inclusions from lower-mantle diamonds, recovered from Brazil and Guinea (Kaminsky et al. 2015). Values of $\Delta \log f_{\text{O}_2}$ of the IW buffer vary from 1.58 to 7.76 logarithmic units (for $T = 1960$ K) (Fig. 2.4). Samples from Juina kimberlites and São Luiz placer deposits form a single set (except one sample from São Luiz), which is understandable, considering their close spatial proximity within the same Juina area and an identical genesis of hosting diamonds. These data demonstrate the linear correlation between $\Delta \log f_{\text{O}_2}$ and fe values varying in a wide range (0.150–0.641), while ferropericlas from Kankan, Guinea, vary almost within the same $\Delta \log f_{\text{O}_2}$ value range, having almost constant fe (0.117–0.167).

Fig. 2.4 Oxygen fugacity values versus $\text{Fe}/(\text{Mg} + \text{Fe})$ values in ferropericlas grains ($P = 25$ GPa; $T = 1960$ K). Trend line demonstrates linear correlation between $\log f_{\text{O}_2}$ and fe in Brazilian samples. FMQ buffer position (IW + 7.87) calculated for 25 GPa and 1960 K using data from Holland et al. (2013). From Kaminsky et al. (2015). ©Elsevier



2.7.3 Oxygen Fugacity Conditions in the Lower Mantle

These results demonstrate wide variations in oxygen fugacity within the lower-mantle region where diamonds are formed. The calculated variations are within a range of more than six logarithmic units ($\Delta = 6.2$), much greater than that suggested previously for the lower mantle ($\Delta = 1.6\text{--}1.7$; Rohrbach and Schmidt 2011; Otsuka et al. 2013).

The $\Delta \log f_{\text{O}_2}$ values are above the IW buffer, demonstrating unexpectedly high oxidation conditions within the lower mantle (Fig. 2.5). In general, $\Delta \log f_{\text{O}_2}$ values for the lower mantle are similar to those of the upper mantle (Woodland and Koch 2003; McCammon and Kopylova 2004; Lazarov et al. 2009; Creighton et al. 2010;

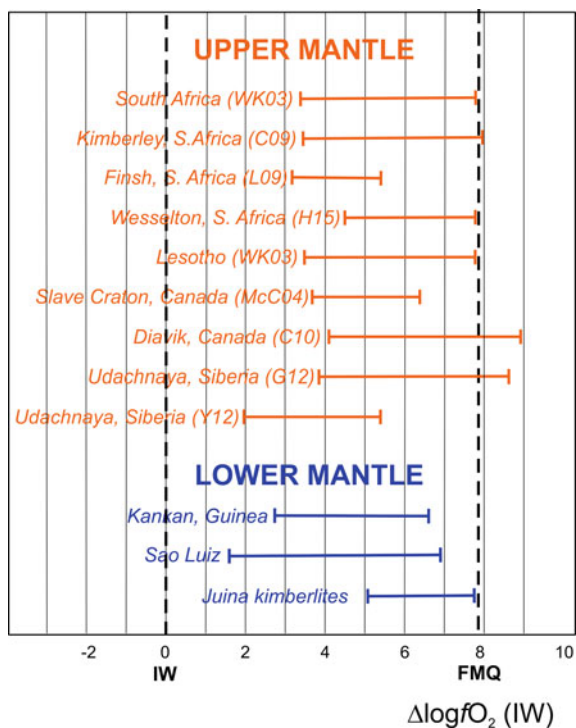


Fig. 2.5 Oxygen fugacity values for lower-mantle ferropericlase compared with the values for garnet from the upper mantle. *IW* position of the iron-wüstite buffer. *FMQ* position of the fayalite-magnetite-quartz buffer. Data on the Kaapvaal Craton in South Africa from Woodland and Koch 2003 (WC03), Lazarov et al. 2009 (L09) and Hanger et al. 2014 (H14). Data on the Slave Craton in Canada from McCandless and Kopylova 2004 (McC04) and Creighton et al. 2010 (C10). Data on the Siberian Craton in Russia from Goncharov et al. 2012 (G12) and Yaxley et al. 2012 (Y12). FMQ buffer position ($\text{IW} + 7.87$) calculated for 25 GPa and 1960 K using data from Holland et al. (2013). From Kaminsky et al. (2015).©Elsevier

Goncharov et al. 2012; Yaxley et al. 2012; Hanger et al. 2014), as has been suggested before (McCammon et al. 2004b).

These data are in agreement with the recent theoretic calculations based on the grounds of the calculated Ni/Fe partition coefficient (Ryabchikov and Kaminsky 2013, 2014). They demonstrate that the typical values of oxygen fugacity in zones of diamond formation in the lower mantle lie between the IW buffer and 3–5 logarithmic units above this level. The processes that operate in the lower mantle can give rise to variation of within several orders of magnitude above the elevated values, which are necessary for the formation of diamond, as compared with common oxygen fugacity levels typical of the lower mantle.

The calculated high oxidation conditions within the lower mantle are confirmed by the presence, in lower-mantle diamonds, of carbonate mineral inclusions (Kaminsky et al. 2009, 2013) and by the existence of magnesioferrite/ Fe^{3+} cluster exsolution in ferropicrinite with its high concentration of Fe^{3+} (Kaminsky et al. 2015). In addition to carbonates, inclusions of free silica have been identified in lower-mantle diamonds as an abundant phase for all known localities (Brazil, Guyana and Canada) (Kaminsky 2012). On the other hand, low oxygen fugacity conditions may also exist within the lower mantle. They are indicated by the presence of the metallic iron + iron carbide association found among inclusions in lower-mantle diamond (Kaminsky and Wirth 2011). Such conditions, with $\Delta\log f_{\text{O}_2}$ values at and below the IW oxygen buffer, may occur in the lowermost lower mantle and D'' layer. The performed calculations by Kaminsky et al. (2015) demonstrate that with an increase in temperature and pressure conditions, the $\Delta\log f_{\text{O}_2}$ values fall and may reach or lie below the IW oxygen buffer. Therefore, the diapason of $\Delta\log f_{\text{O}_2}$ values within the entire sequence of the lower mantle may reach ten logarithmic units, varying from below the IW buffer to the FMQ buffer values.

2.8 Conclusions

Geophysical models, based on the pyrolitic or chondritic average compositions of the Earth's mantle, demonstrate gradual changes in seismic wave velocities, density, temperature and other physical properties within the lower mantle. However, so far, none of the lower-mantle model compositions (pyrolite, CI-chondrite, 'cosmic') fully fits the data on seismic velocities. They all show a significant mismatch, particularly in the lower part of the lower mantle, observing compositional differences between the lower and upper mantle.

Of particular interest are indications of the enrichments of the lower mantle in SiO_2 , in comparison with the pyrolitic upper mantle. Such indications were obtained from both re-examination of the seismic profile (Matas et al. 2007) and analysis of the density profile (Ricolleau et al. 2008, 2009) within the lower mantle.

Despite some uncertainties in the PREM, we used this model in all of our further constructions. All mismatches, in our opinion, are caused by the non-pyrolitic

composition of the lower mantle, which is confirmed by data on natural mineral association from the lower mantle.

The oxygen fugacity $\Delta \log \text{Emphasis}>\text{O}_2$ values for the lower mantle are similar to those of the upper mantle. The entire sequence of the lower mantle may reach ten logarithmic units, varying from below the IW buffer to the FMQ buffer values.

References

- Anderson, D. L. (1983). Chemical composition of the Mantle. *Journal of Geophysical Research*, 88, B41–B52. doi:[10.1029/Jb088is01p00b41](https://doi.org/10.1029/Jb088is01p00b41)
- Anderson, D. L. (1989). *Theory of the Earth*. Oxford: Blackwell.
- Andrault, D., Bolfan-Casanova, N., Nigro, G. L., Bouhifd, M. A., Garbarino, G., & Mezouar, M. (2011). Solidus and liquidus profiles of chondritic mantle: Implication for melting of the Earth across its history. *Earth and planetary science letters*, 304(1), 251–259.
- Badro, J., Fiquet, G., Guyot, F., Rueff, J. P., Struzhkin, V. V., Vankó, G., et al. (2003). Iron partitioning in Earth's mantle: Toward a deep lower mantle discontinuity. *Science*, 300(5620), 789–791.
- Bass, J. D., & Anderson, D. L. (1984). Composition of the upper mantle: Geophysical tests of two petrological models. *Geophysical Research Letters*, 11, 229–232.
- Berry, A. J., Yaxley, G. M., Hanger, B. J., Woodland, A. B., De Jonge, M. D., Howard, D. L., et al. (2013). Quantitative mapping of the oxidative effects of mantle metasomatism. *Geology*, 41, 683–686.
- Brown, J. M., & Shankland, T. J. (1981). Thermodynamic parameters in the Earth as determined from seismic profiles. *Geophysical Journal of the Royal Astronomical Society*, 66, 579–596.
- Bullen, K. E. (1942). The density variation of the Earth's central core. *Bulletin of the Seismological Society of America*, 30, 235–250.
- Bullen, K. E. (1950). An Earth model based on compressibility-pressure hypothesis. *Monthly Notices of the Royal Astronomical Society Supplement*, 6, 50–59.
- Creighton, S., Stachel, T., Eichenberg, D., & Luth, R. (2010). Oxidation state of the lithospheric mantle beneath Diavik diamond mine, central Slave craton, NWT, Canada. *Contributions to Mineralogy and Petrology*, 159(5), 645–657.
- Da Silva, C. R. S., Wentzcovitch, R. M., Patel, A., Price, G. D., & Karato, S. I. (2000). The composition and geotherm of the lower mantle: constraints from the elasticity of silicate perovskite. *Physics of the Earth and Planetary Interiors*, 118, 103–109.
- Davis, F. A., Tangeman, J. A., Tenner, T. J., & Hirschmann, M. M. (2009) The composition of KLB-1 peridotite. *American Mineralogist*, 94, 176–180.
- Deuss, A., & Woodhouse, J. (2001). Seismic observations of splitting of the mid-transition zone discontinuity in the Earth's mantle. *Science*, 294, 354–357.
- Deuss, A., Redfern, S. A. T., Chambers, K., & Woodhouse, J.H. (2006). The nature of the 660-kilometer discontinuity in Earth's mantle from global seismic observations of PP precursors. *Science*, 311, 198–201.
- Dziewonski A., & Anderson D. (1981) Preliminary reference Earth model. *Physics of Earth and Planetary Interiors*, 25, 297–356. doi:[10.1016/0031-9201\(81\)90046-7](https://doi.org/10.1016/0031-9201(81)90046-7)
- Fiquet, G., Auzende, A. L., Siebert, J., Corgne, A., Bureau, H., Ozawa, H., et al. (2010). Melting of peridotite to 140 Gigapascals. *Science*, 329, 1516–1518. doi:[10.1126/science.1192448](https://doi.org/10.1126/science.1192448)
- Foley, S. F. (2011). A reappraisal of redox melting in the Earth's mantle as a function of tectonic setting and time. *Journal of Petrology*, 52(7), 1363–1391.
- Frost, D. J., & McCammon, C. A. (2008). The redox state of Earth's mantle. *Annual Review of Earth and Planetary Sciences*, 36, 389–420.

- Goncharov, A. G., Ionov, D. A., Doucet, L. S., & Pokhilenko, L. N. (2012). Thermal state, oxygen fugacity and C-O-H fluid speciation in cratonic lithospheric mantle: New data on peridotite xenoliths from the Udachnaya kimberlite, Siberia. *Earth and Planetary Science Letters*, 357–358, 99–110.
- Hanger, B. J., Yaxley, G. M., Berry, A. J., & Kamenetsky, V. S. (2014). Relationships between oxygen fugacity and metasomatism in the Kaapvaal subcratonic mantle, represented by garnet peridotite xenoliths in the Wesselson kimberlite, South Africa. *Lithos*, 212–215, 443–452. doi:[10.1016/j.lithos.2014.09.030](https://doi.org/10.1016/j.lithos.2014.09.030)
- Hart, S. R., & Zindler A. (1986). In search of a bulk-Earth composition. *Chemical Geology*, 57(3–4), 247–267.
- Hirose, K. (2002). Phase transitions in pyrolitic mantle around 670-km depth: Implications for upwelling of plumes from the lower mantle. *Journal of Geophysical Research*, 107(B4) 2078. doi:[10.1029/2001JB000597](https://doi.org/10.1029/2001JB000597)
- Holland, K. G., & Ahrens, T. J. (1997) Melting of $(\text{Mg,Fe})_2\text{SiO}_4$ at the Core-Mantle Boundary of the Earth. *Science*, 275, 1623–1625.
- Holland, T. J. B., Hudson, N. F. C., Powell, R., & Harte, B. (2013). New thermodynamic models and calculated phase equilibria in NCFMAS for basic and ultrabasic compositions through the transition zone into the uppermost lower mantle. *Journal of Petrology*, 54, 1901–1920.
- Hyung, E., Huang, S., Petaev, M. I., & Jacobsen, S. B. (2016). Is the mantle chemically stratified? Insights from sound velocity modeling and isotope evolution of an early magma ocean. *Earth and Planetary Science Letters*, 440(2016) 158–168. doi:[10.1016/j.epsl.2016.02.001](https://doi.org/10.1016/j.epsl.2016.02.001)
- Irifune, T., Shinmei, T., McCammon, C. A., Miyajima, N., Rubie, D. C., & Frost D. J. (2010). Iron partitioning and density changes of pyrolite in Earth's lower mantle. *Science*, 327(5962) 193–195.
- Ito, E., & Katsura, T. (1989). A temperature profile on the mantle transition zone. *Geophysical Research Letters*, 16(5), 425–428.
- Javoy, M. (1995). The integral enstatite chondrite model of the Earth. *Geophysical Research Letters*, 22(16), 2219–2222.
- Jeanloz, R., & Knittle, E. (1989). Density and composition of the lower mantle. *Philosophical Transactions of the Royal Society of London*, A328(1599), 377–389. doi:[10.1098/rsta.1989.0042](https://doi.org/10.1098/rsta.1989.0042)
- Kaminsky, F. V. (2012). Mineralogy of the lower mantle: A review of 'super-deep' mineral inclusions in diamond. *Earth-Science Reviews*, 110(1–4), 127–147.
- Kaminsky, F. V., & Wirth, R. (2011). Iron carbide inclusions in lower-mantle diamond from Juina, Brazil. *Canadian Mineralogist* 49(2), 555–572.
- Kaminsky, F., Wirth, R., Matsyuk, S., Schreiber, A., & Thomas, R. (2009). Nyerereite and nahcolite inclusions in diamond: Evidence for lower-mantle carbonatitic magmas. *Mineralogical Magazine*, 73(5), 797–816.
- Kaminsky, F. V., Wirth, R., & Schreiber, A. (2013) Carbonatitic inclusions in Deep Mantle diamond from Juina, Brazil: New minerals in the carbonate-halide association. *Canadian Mineralogist*, 51(5), 447–466.
- Kaminsky, F. V., Ryabchikov, I. D., McCammon, C., Longo, M., Abakumov, A. M., Turner, S., et al. (2015). Oxidation potential in the Earth's lower mantle as recorded from ferropericlasite inclusions in diamond. *Earth and Planetary Science Letters*, 417, 49–56.
- Katsura, T., Yoneda, A., Yamazaki, D., Yoshino, T., & Ito E. (2010). Adiabatic temperature profile in the mantle. *Physics of the Earth and Planetary Interiors*, 183, 212–218. doi:[10.1016/j.pepi.2010.07.001](https://doi.org/10.1016/j.pepi.2010.07.001)
- Kennett, B. L. N., & Engdahl, E. R. (1991) Traveltimes for global earthquake location and phase identification. *Geophysical Journal of International*, 105, 429–465.
- Kennett, B., Engdahl, E., & Buland, R. (1995). Constraints on seismic velocities in the Earth from traveltimes. *Geophysical Journal of International*, 122, 108–124.
- Kirby, S. H., Stein, S., Okal, E. A., & Rubie D. C. (1996). Metastable mantle phase transformations and deep earthquakes in subducting oceanic lithosphere. *Reviews of Geophysics*, 34(2), 261–306.

- Kustowski, B., Ekström, G., & Dziewoński A. M. (2008). Anisotropic shear-wave velocity structure of the Earth's mantle: A global model. *Journal of Geophysical Research*, 113, B06306. doi:[10.1029/2007JB005169](https://doi.org/10.1029/2007JB005169)
- Lazarov, M., Woodland, A. B., & Brey, G. P. (2009). Thermal state and redox conditions of the Kaapvaal mantle: A study of xenoliths from the Finsch mine, South Africa. *Lithos*, 112S, 913–923.
- Lin, J-F., Speciale, S., Mao, Z., & Marquardt, H. (2013). Effects of the electronic spin transitions of iron in lower mantle minerals: Implications for deep mantle geophysics and geochemistry. *Reviews of Geophysics*, 51(2), 244–275.
- McCammon, C. (1997). Perovskite as a possible sink for ferric iron in the lower mantle. *Nature*, 387, 694–696.
- McCammon, C., & Kopylova, M. G. (2004). A redox profile of the Slave mantle and oxygen fugacity control in the cratonic mantle. *Contributions to Mineralogy and Petrology*, 148(1), 55–68.
- McCammon, C., Hutchison, M. T., & Harris J. W. (1997) Ferric iron content of mineral inclusions in diamonds from São Luiz: A view into the lower mantle. *Science*, 278(5337), 434–436.
- McCammon, C. A., Lauterbach, S., Seifert, F., Langenhorst, F., & van Aken, P. A. (2004a). Iron oxidation state in lower mantle mineral assemblages. I. Empirical relations derived from high-pressure experiments. *Earth and Planetary Science Letters*, 222(2), 435–449.
- McCammon, C. A., Stachel, T., & Harris, J. W. (2004b). Iron oxidation state in lower mantle mineral assemblages. II. Inclusions in diamonds from Kankan, Guinea. *Earth and Planetary Science Letters*, 222(2), 423–434.
- Matas, J., Bass, J. D., Ricard, Y., Mattern, E., & Bukowinsky, M. S. (2007). On the bulk composition of the lower mantle: predictions and limitations from generalized inversion of radial seismic profiles. *Geophysical Journal International* 170, 764–780.
- McDonough, W. F., & Sun S. S. (1995). The composition of the Earth. *Chemical Geology*, 120(3–4), 223–253.
- Morgan, J. W., & Anders E. (1980). Chemical composition of Earth, Venus, and Mercury. *Proceedings of the National Academy Science USA*, 77(12), 6973–6977. doi:[10.1073/pnas.77.12.6973](https://doi.org/10.1073/pnas.77.12.6973)
- Murakami, M., Ohishi, Y., Hirao, N., & Hirose K. (2012). A perovskitic lower mantle inferred from high-pressure, high-temperature sound velocity data. *Nature*, 485(7396), 90–94.
- Nomura, R., Hirose, K., Uesugi, K., Ohishi, Y., Tsuchiyama, A., Miyake, A., et al. (2012). Low core-mantle boundary temperature inferred from the solidus of Pyrolite. *Science*, 343, 523–525.
- Otsuka, K., Longo, M., McCammon, C. A., & Karato, S.-i. (2013). Ferric iron content of ferropericlase as a function of composition, oxygen fugacity, temperature and pressure: Implications for redox conditions during diamond formation in the lower mantle. *Earth and Planetary Science Letters*, 365, 7–16.
- Ricolleau, A., Fiquet, G., Addad, A., Menguy, N., Vanni, C., Perrillat, J.-P., et al. (2008). Analytical transmission electron microscopy study of a natural MORB sample assemblage transformed at high pressure and high temperature. *American Mineralogist*, 93, 144–153. doi:[10.2138/am.2008.2532](https://doi.org/10.2138/am.2008.2532)
- Ricolleau, A., Fei, Y., Cottrell, E., Watson, H., Deng, L., Zhang, L., et al. (2009). Density profile of pyrolite under the lower mantle conditions. *Geophysical Research Letters*, 36, L06302. doi:[10.1029/2008GL036759](https://doi.org/10.1029/2008GL036759)
- Ringwood, A. E. (1975). Composition and petrology of the Earth's mantle. (p. 618). New York: McGraw-Hill.
- Rohrbach, A., & Schmidt, M. W. (2011). Redox freezing and melting in the Earth's deep mantle resulting from carbon–iron redox coupling. *Nature*, 472 209–214.
- Ryabchikov, I. D., & Kaminsky, F. V. (2013). Redox potential of diamond formation processes in the lower mantle. *Geology of Ore Deposits*, 55(1), 1–12.

- Ryabchikov, I. D., & Kaminsky, F. V. (2014). Physico-chemical parameters of material in mantle plumes: Evidence from the thermodynamic analysis of mineral inclusions in sublithospheric diamonds. *Geochemistry International*, 52(11), 963–971.
- Shahnas, M. H., Peltier, W. R., Wu, Z., & Wentzcovitch, R. (2011). The high-pressure electronic spin transition in iron: Potential impacts upon mantle mixing. *Journal of Geophysical Research*, 116, B08205. DOI:[10.1029/2010JB007965](https://doi.org/10.1029/2010JB007965)
- Shen, Y., Solomon, S. C., Bjarnson, I. T., & Wolfe, C. J. (1998). Seismic evidence for the lower-mantle origin of the Iceland plume. *Nature*, 395, 62–65.
- Simmons, N. A., Forte, A. M., Boschi, L., & Grand S. P. (2010). GyPSuM: A joint tomographic model of mantle density and seismic wave speeds. *Journal of Geophysical Research*, 115, B12310, doi:[10.1029/2010JB007631](https://doi.org/10.1029/2010JB007631)
- Simmons, N. A., Forte, A. M., Boschi, L., & Grand, S. P. (2010). GyPSuM: A joint tomographic model of mantle density and seismic wave speeds. *Journal of Geophysical Research*, 115, B12310. doi:[10.1029/2010JB007631](https://doi.org/10.1029/2010JB007631)
- Stacey, F. D., & Davis, P. M. (2008). *Physics of the Earth*. (4th ed., p. 532). Cambridge: Cambridge University Press.
- Stagno, V., Ojwang, D. O., McCammon, C. A., & Frost, D. J. (2013). The oxidation state of the mantle and the extraction of carbon from Earth's interior. *Nature*, 493, 84–88.
- Stixrude, L., & Lithgow-Bertelloni, C. (2012). Geophysics of chemical heterogeneity in the mantle. *Annual Review of Earth and Planetary Science*, 40, 569–595.
- Stixrude, L., de Koker, N., Sun, N., Mookherjee, M., & Karki, B.B. (2009). Thermodynamics of silicate liquids in the deep Earth. *Earth and Planetary Science Letters*, 278, 226–232. doi:[10.1016/j.epsl.2008.12.006](https://doi.org/10.1016/j.epsl.2008.12.006)
- Sun, N., Mao, Z., Yan, S., Lin, J. F., Wu, X., & Prakapenka, V. B. (2016). Confirming a pyrolytic lower mantle using self-consistent pressure scales and new constraints on CaSiO₃-perovskite. *Journal of Geophysical Research*, 121(7), 4876–4892. doi:[10.1002/2016JB013062](https://doi.org/10.1002/2016JB013062)
- Tesoniero, A., Auer, L., Boschi, L., & Cammarano, F. (2015). Hydration of marginal basins and compositional variations within the continental lithospheric mantle inferred from a new global model of shear and compressional velocity. *Journal of Geophysical Research: Solid Earth*, 120 (11), 7789–7813. doi:[10.1002/2015JB012026](https://doi.org/10.1002/2015JB012026)
- Turcotte, D. L., & Schubert, G. (2002). *Geodynamic*, (2nd ed., p. 456). Cambridge: Cambridge University Press.
- Wang, X. L., Tsuchiya, T., & Hase, A. (2015). Computational support for a pyrolytic lower mantle containing ferric iron. *Nature Geoscience*, 0, 556–559. doi:[10.1038/ngeo2458](https://doi.org/10.1038/ngeo2458)
- Williams, Q., & Knittle, E. (2005). The uncertain major element bulk composition of Earth's mantle. In: R.D. Van der Hilst, J. Bass, J. Matas and J. Trampert (Eds.), *Earth's deep mantle: Structure, composition and evolution*. (pp. 189–202). Washington DC: AGU.
- Wood, B. J., Bryndzia, L. T., & Johnson, K. E. (1990). Mantle oxidation state and its relationship to tectonic environment and fluid speciation. *Science*, 248, 337–344.
- Woodland, A. B., & Koch, M. (2003). Variation in oxygen fugacity with depth in the upper mantle beneath the Kaapvaal craton, Southern Africa. *Earth and Planetary Science Letters*, 214, 295–310.
- Yaxley, G. M., Berry, A. J., Kamenetsky, V. S., Woodland, A. B., & Golovin, A. V. (2012) An oxygen fugacity profile through the Siberian Craton—Fe K-edge XANES determinations of Fe³⁺/ΣFe in garnets in peridotite xenoliths from the Udachnaya East kimberlite. *Lithos*, 140–141, 142–151.
- Zhang, S., Cottar, S., Liu, T., Stackhouse, S., & Militzer, B. (2016). High-pressure, temperature elasticity of Fe- and Al-bearing MgSiO₃: Implications for the Earth's lower mantle. *Earth and Planetary Science Letters*, 434, 264–273. doi:[10.1016/j.epsl.2015.11.030](https://doi.org/10.1016/j.epsl.2015.11.030)

<http://www.springer.com/978-3-319-55683-3>

The Earth's Lower Mantle
Composition and Structure

Kaminsky, F.

2017, XIII, 331 p. 150 illus., 131 illus. in color.,
Hardcover

ISBN: 978-3-319-55683-3